doi:10.14311/ppt.2017.2.186
Plasma Physics and Technology **4**(2):186–189, 2017

VACUUM ARC ION FLUX FROM VACUUM INTERRUPTER CONTACT GAP

M. Kurrat

Technische Universitaet Braunschweig, Institute for High Voltage Technology and Electrical Power Systems Schleinitzstrasse 23, 38106 Braunschweig, Germany

m.kurrat@tu-braunschweig.de

Abstract. Dielectric properties of vacuum interrupters are influenced by metal vapour deposition on the inner ceramic surfaces. Therefore these surfaces are partly protected by shield electrodes. The metal vapour originates from the vacuum arc in the contact gap during switching off process. Metal layer thickness on ceramics after switching operations were measured by Gramberg [1] and the negative effect on dielectric performance was demonstrated. In this paper we address the principle transport process of metal vapour in vacuum interrupters. Düning [2] and Beilis [3] performed ion flux measurements from vacuum arcs. We regard experiments with 5 kA effective arc current. There seems to be experimental evidence that the final particle transport onto the ceramic surface within a shield gap can be explained by particle tracing. The measured deposited layer thickness is taken as quantity to validate vapour densities and transport processes in vacuum interrupters.

Keywords: vacuum interrupter, vacuum arc, ion flux, metal vapour, layer deposition, particle tracing.

1. Introduction

The contact system of a vacuum interrupter is surrounded by the main shield made of copper. Breaking currents generates a metal vapour arc between the contacts (fig. 1). This arc emits metal vapour into the vacuum chamber at increasing gas pressure. After cooling the metal vapour condenses on main and end shields, but also on the inner surface of the ceramic insulator. The deposited conductive layers bridge partly the dielectric gaps between the shields (fig. 1, layer length L). The dielectric strength is decreased by shortening the dielectric gap and a flash over across the inner ceramic surface may result by overvoltage incidents (fig. 1).

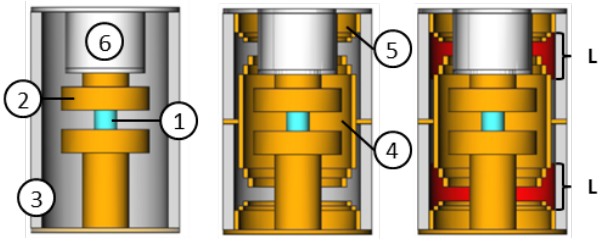

Figure 1. Metal vapour arc (1) between contacts (2) in a ceramic tube (3) without and with main (4) and end (5) condensation shields / metal vapour deposition through inter shield gap (L) / bellow (6).

To investigate the reduction of dielectric strength, vacuum interrupter with simple shield geometry were tested. High numbers of short circuit breaking operations were done in a test circuit. After breaking tests the significant dielectric performance reduction was evaluated by lightning impulse tests [1]. To improve the knowledge about the metal vapour layer deposition process the vacuum interrupters were opened after the tests. The layer position and thickness were measured. Figure 2 shows the layer thickness on the ceramic surface of the inter shield gap after 40 breaking operations at 5 kA.

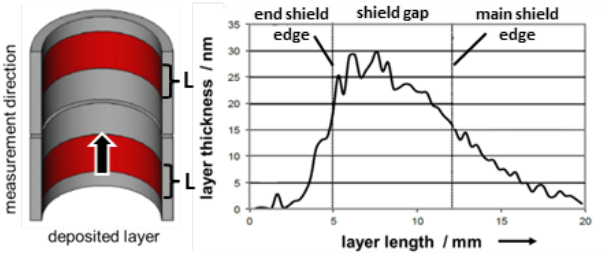

Figure 2. Measurement of deposition layer L thickness on ceramics from end shield to main shield (arrow).

The vertical lines mark the position of the inter electrode gap between position 5 and 12 mm. In between the thickness of the deposition layer reached the maximum value. But the deposition layer was also found behind the shields. The thickness decreases with increasing distance from the inter shield gap.

2. Particles Generation and Transport

The metal vapour flux from the arc between the contacts to the main shield is generated by the arc pressure. But the question arises what kind of transport mechanisms controls the deposition process behind the shields. Is it still a diffusion process and what is about the mean free path length? A stepwise approach for a simple calculation will be proposed in turn below. The particles are generated in the arc and released. Secondly the particles diffuse into the whole volume

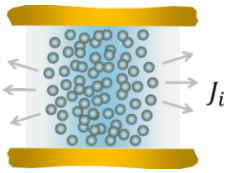

Figure 3. Radial ion current density leaving the thermal arc plasma.

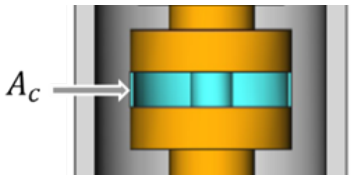

Figure 4. Cylindrical control area A_c for radial ion flux calculation.

creating a gas pressure in the vacuum chamber. The last step is the deposition process between main and end shield.

2.1. Ion Flux from Contact Gap

Rusteberg [4] and Düning [2] measured the ion flux from a diffuse mode vacuum arc with currents up to 10 kA. Ion current densities and ion energies were measured with a retarded field analyzer. For the calculations they assumed thermal arc plasma completely ionized and dominated by ion collisions. In result scattered ions with radial velocity components leave the contact gap with an ion current density J_i (fig. 3).

The calculated radial ion current density leaving the contact gap refers to a cylindrical control area A_c around the contact gap as shown in fig. 4.

Some more quantities can be deduced from the measured quantities [5] using equations (1) and (2). The measured ion energies allow the calculation of the ion velocities v_i. And the measured ion current densities J_i include the information about the ion densities n_i regarding ion charge q.

$$J_\mathrm{i} = n_\mathrm{i}\, v_\mathrm{i}\, q \tag{1}$$

$$W_\mathrm{i} = \frac{1}{2}\, m_\mathrm{i}\, {v_\mathrm{i}}^2 \tag{2}$$

The calculated ion densities of the radial flux increase with the arc current up to values of $10^{19}\,\mathrm{m}^{-3}$ as shown in fig. 5.

The maximum ion energies were observed at lower short circuit currents. Thermal ion energies at high arc currents yield high velocities about $v_\mathrm{i} = 10^4\,\mathrm{m\,s}^{-1}$. High ion densities result in a low mean free path λ_i in the mm range calculated for high arc currents with equation (3).

$$\lambda_\mathrm{i} = v_\mathrm{i}/(c_0\, n_\mathrm{i}),\ c_0 = 8 \cdot 10^{-13}\,\mathrm{m^3 s^{-1}}. \tag{3}$$

2.2. Axial Collisional Transport

The burning arc emits continuously ions from the contact gap into the vacuum chamber through the

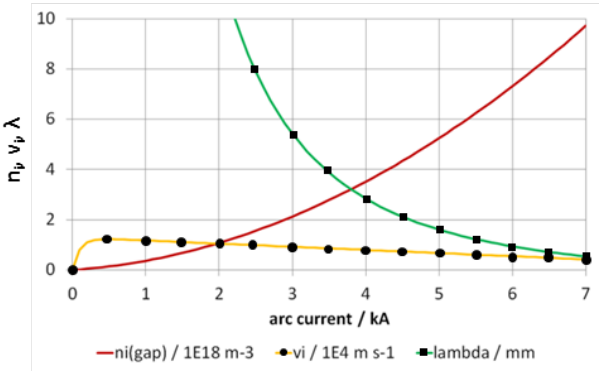

Figure 5. Ion density n_i, ion velocity v_i and mean free path lengths λ_i of the ion flux through the control area calculated from measurements.

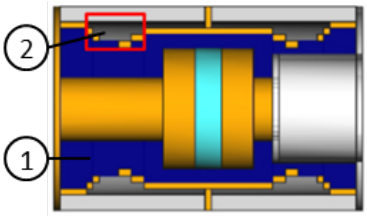

Figure 6. Chamber volume (1) with constant metal vapour particle density and inter shield gap volumes (2, red box).

control area A_c. The total ion number escaping from the arc gap within one time step Δt is given by eq. (4).

$$N_\mathrm{i} = n_\mathrm{i}(\mathrm{gap}) \cdot v_\mathrm{i}(\mathrm{gap}) \cdot A_\mathrm{c} \cdot \Delta t \tag{4}$$

To obtain a particle density in the vacuum chamber the total number of ions from the arc gap is divided by the chamber volume V_chamber as shown by eq. (5).

$$n_\mathrm{i}(\mathrm{chamber}) = N_\mathrm{i}/V_\mathrm{chamber} \tag{5}$$

The dark blue volume in fig. 6 without electrode gap and inter shield gaps is taken as chamber volume V_chamber filled by metal vapour. It is assumed that the initial ion flux is distributed as metal vapour over the chamber volume within one time step of 0.1 ms. The distribution process is not completely understood but some physical aspects are described in turn. The positive ion flux is directed to the main shield. When the ions hit the copper shield, they are neutralized by electrons. Due to the ionization energy further electrons may be liberated from the metal (secondary electron emission) and further atoms are neutralised. The low sticking coefficient about 2 % may be a result of this surface process. In addition the main shield is charged by the ion flux and the positive ions are retarded and do not reach the shield. In result a diffusion process is assumed and electric forces are not regarded.

With the arc current dependence of the measured ion flux shown in fig. 5 the mean density of the metal vapour in the vacuum chamber can be calculated for the sinusoidal arc current. The particle density in the

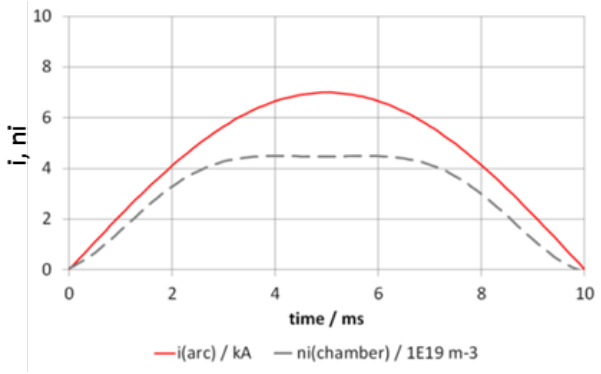

Figure 7. Time curves of arc current and particle densities in the chamber, $\Delta t = 0.1$ ms.

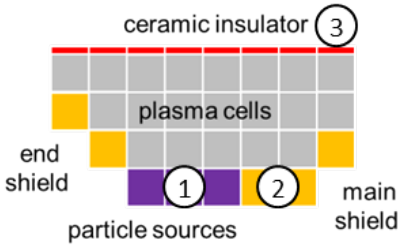

Figure 8. Discretisation of inter shield gap volume with particle source elements (1), shield elements (2), insulator surface elements (3).

vacuum chamber reaches $10^{-19}\,\mathrm{m}^{-3}$ calculated with an integration time step of 0.1 ms. The mean free path has accordingly a length in the mm range. The particle density reduction through sticking to metal surfaces during one time step is neglected. The total particle density in the vacuum chamber is shown in fig. 7 for one half sine of a 5 kA arc current (rms). The high initial ion velocity of $10^4\,\mathrm{m\,s}^{-1}$ supports the metal vapour diffusion through the whole vacuum chamber within one time step.

2.3. Radial Transport in Shield Gap

The last transport path is the gap between the shields. The regarded transport volume is marked with a red box in fig. 6. The metal vapour density in the chamber volume in front of the shield gap is given in fig. 8 as "particle source" within one time step. To calculate the particle number which are collected by the ceramic insulator surfaces a rough two-dimensional discretisation of the inter shield gap volume is applied as shown in fig. 8. Depending on the mean free path two transport processes are possible: Diffusion or crossing the inter shield gap without collisions.

2.3.1. Collisonal Transport

The first transport process test assumes diffusion as predominant. The two dimensional partial differential equation (6) is solved numerically by difference equations with total particle numbers N in cells of

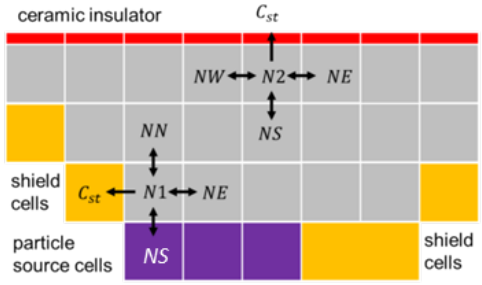

Figure 9. Two dimensional cell model for calculation of particle transport by diffusion.

constant volumes and diffusion coefficient D.

$$\frac{\partial N}{\partial t} = D \cdot \left[\frac{\partial^2 N}{\partial x^2} + \frac{\partial^2 N}{\partial y^2} \right[\qquad (6)$$

The particle densities of the particle source cells are given in equation 5. The particle distribution is calculated within one time step $\Delta t = 0.1$ ms with 5 iterations of 5-points difference equations (compass notation). The shield cells and insulator cells are particle drains and the sticking coefficients C_{st} determine the particle collection of these cells. The particle numbers $N1$ and $N2$ in the example cells in fig. 9 are given in the iteration equations (7), (8).

$$N1 = (NN + NE + NS)/(3 + C_{\mathrm{st}}(\mathrm{shield})) \qquad (7)$$

$$N2 = (NE + NS + NW)/(3 + C_{\mathrm{st}}(\mathrm{ceramic})) \qquad (8)$$

The cell definitions are shown in fig. 9 and they are applied at every volume cell connected to a shield cell or a ceramic cell. Due to the low sticking coefficient C_{st} only a small part of particles is collected from the insulator cells.

2.3.2. Particle Tracing

The second transport process test assumes low particle densities and no particle collisions in the shield gap. Particles from the vacuum chamber volume fly from the source cells i directly to the ceramic insulator cells j. For each insulator cell a receiving coefficient $R_{\mathrm{c}}(i,j)$ is calculated within one time step according to the geometry. fig. 10 shows the particle tracing lines from the centre of the source cells to the receiving insulator cells. The given receiving coefficients $R_{\mathrm{c}}(i,j)$ for the insulator cells show the geometrical dependance examplarily. The particle numbers in each insulator cell j is the sum in equation (9) over all plasma source cells i. But only a small part of particles is adsorbed from the insulator surface due to the low sticking coefficient.

$$N_j(\mathrm{insulator}) = \sum_i R_{\mathrm{c}}(i,j) \cdot N_i(\mathrm{source}) \qquad (9)$$

2.4. Calculation of Layer Thickness

The numbers of metal particles reaching the insulator surface cells are summed up during one half sinewave

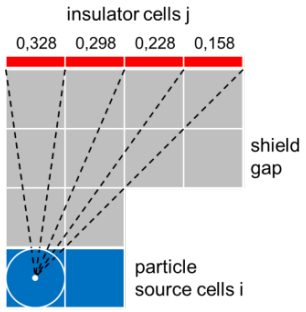

Figure 10. Particle tracing model with receiving coefficients of the red ceramic insulator cells on top.

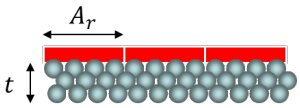

Figure 11. Insulator cell with surface area A_r and metal vapour layer thickness t.

of arc current. A low sticking coefficient of copper on ceramic surface about 2 % is assumed. The layer thickness t is calculated due to the particle number per surface area A_r as shown in fig. 11. The mass of the layer is given by the number of particles and the atomic mass unit $u = 63$. The deposited layer thickness t is calculated by the insulator cell surface area A_r and the specific density $\rho = 8.9\,\mathrm{g\,cm^{-3}}$ of copper as given by equations (10), (11).

$$m = N \cdot u \cdot 1.66 \cdot 10^{-24}\,\mathrm{g} \tag{10}$$

$$t = m/(\rho \cdot A_r) \tag{11}$$

3. Results

The diffusion approach assumes a low average free path length and therefore fluid dynamics are applicable. Figure 12 shows the layer thickness after 40 breaking operations at 5 kA arc current. The curve shows the measured thickness values of 30 nm with a steep decrease behind the end shield and a broader one behind the main shield. The calculated layer thickness for the insulator cells are given as bars. The calculated values exhibit a broad distribution of layer thickness behind the shields.

The particle tracing approach assumes a collisional free transport in the shield gap. The bar graph in fig. 13 shows the layer thickness of the insulator cells obtained by free particle flight through the inter shield gap. The bar distribution is quite similar to the measured distribution curve. The layer thickness is influenced by the "optical properties". The distribution exhibits a shadow effect of the end and main shield.

4. Conclusion

A simple model calculation for the deposition of metal vapour is compared to experimental results. The following are found.

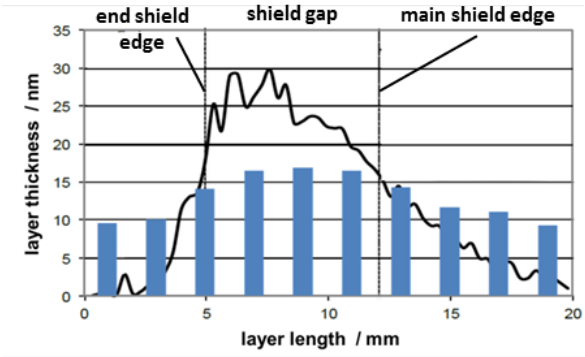

Figure 12. Measured (line) and calculated (bars) vapour layer thickness by diffusion.

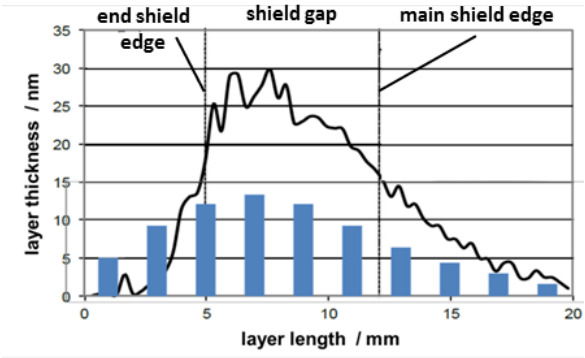

Figure 13. Measured (line) and calculated (bars) vapour layer thickness by particle tracing.

- ☐ The ion flux from vacuum arc is one important source for metal vapour emission into the vacuum chamber.
- ☐ The ions are partly or completely converted into neutrals and are distributed over the vacuum chamber volume by diffusion.
- ☐ It seems to be a free particle flight in the inter shield gap to the insulator surface which shows the measured shadowing effect of the shields.
- ☐ The calculated layer thickness with low sticking coefficient about 2 % agrees quite well with measured values.

References

[1] I. Gramberg et al. Investigations of copper chrome coatings on vacuum circuit breaker ceramics. *IEEE Trans. Plasma Science*, 41(8):2074–2080, 2013. doi:10.1109/TPS.2013.2273260.

[2] G. Düning and M. Lindmayer. Energy of ions in vacuum arcs. In *Int. Symp. Discharges and El. Insul. in Vacuum, ISDEIV*, Xi'an, 2000.

[3] I. Beilis et al. Measurement of ion flux as a function of background gas pressure. *IEEE Trans. Plasma Science*, 35(4):973–979, 2007. doi:10.1109/TPS.2007.896751.

[4] C. Rusteberg. Plasma parameters in vacuum arcs. Phd Thesis (in German), TU Braunschweig, 1995.

[5] M. Kurrat. Plasma diagnostics for vacuum arcs. In *Symp. on Physics of Switching Arc (FSO)*, Nove Mesto, Tschechien, 2009.